

Dynamics and Structural Transformations of Carbon Onion-Like under High-Velocity Impacts

M. L. Pereira Júnior^a, W. F. da Cunha^a, R. T. de Sousa Junior^b, G. D. Amvame Nze^b,
D. S. Galvão^b, L. A. Ribeiro Júnior^{*a}

^a*Institute of Physics, University of Brasília, Brasília 70919-970, Brazil.*

^b*Department of Electrical Engineering, University of Brasília 70919-970, Brazil.*

^c*Applied Physics Department, University of Campinas, Campinas, São Paulo, Brazil.*

^d*Center for Computing in Engineering and Sciences, University of Campinas, Campinas, São Paulo, Brazil.*

Abstract

Carbon nano-onions (CNO) are multi-shell fullerenes. In the present work, we used fully atomistic reactive (ReaxFF) molecular dynamics simulations to study the dynamics and structural transformations of CNO structures under high-velocity impacts against a fixed and rigid substrate. We considered single and multi-shell CNO (up to six shells) and at different impact velocities (from 2 up to 7 Km/s). Our results indicated three regimes formed after the CNO impact: slightly deformed CNO (quasi-elastic collision, below 2.0 Km/s), collapsed CNO (inelastic collisions, between 3.0 and 5.0 Km/s) forming a diamondoid-like core, and fragmented CNO yielding linear atomic carbon chains (above 5.0 Km/s). We also discussed the dynamical reconfiguration of carbon-carbon bonds during the collision process. The impact of CNO against the substrate yielded sp^3 -like bond types for all the used initial velocities. At intermediate velocities (between 3.0 and 5.0 Km/s), the inelastic collision forms diamondoid-like cores by converting a substantial quantity of sp^2 bonds into sp^3 ones. In the high velocities regime, the total number of sp^1 , sp^2 , and sp^3 bonds tend to be similar.

*Corresponding author. E-mail: ribeirojr@unb.br (Luiz Antônio Ribeiro Júnior). Tel: +55 61 3107-7700.

1. Introduction

Different types of carbon-based materials have been the subject of great interest from the scientific community due to their unique properties and potential applications [1, 2]. As a result, a substantially increased understanding of systems as diverse as conjugated polymers [3], carbon nanotubes [4], graphene nanoribbons [5], and fullerenes [6] has been achieved. Studies on their structural and electronic properties from both experimental [7–11] and theoretical [12–15] points of view stand out. These features are considered crucial for improving electrochemical energy storage [16, 17] and conversion [18, 19] processes in the electronics field.

The fullerenes discovery in the early 80s [4] triggered the synthesis of a novel carbon allotrope based on C_{60} in the 90s. Ugarte reported multilayered fullerenes by working with curved graphitic networks, today known as Carbon Nano-Onions (CNO) [20]. These systems exhibit a unique combination of structural and electronic properties [21]. CNO are quasi-spherical nanostructures composed of multiple enclosed concentric fullerene shells (in a close analogy to the layers of an actual onion, see Figure 1) [21]. Diamond-like core structures have also been observed [22]. These systems present high electrical conductivity levels and a large surface area when contrasted with other nanomaterials [21]. Their relatively easy synthesis provides a level of controllability that allows efficient functionalization procedures [23, 24]. Such properties have made CNO good candidates for a wide range of applications, such as biological imaging and sensing [25, 26], environmental remediation [27, 28], electronics (as batteries, capacitors, fuel cells, and terahertz-shielding devices) [23, 29], catalysts [30], tribology [31], optical limiting [32], and molecular junctions in STM [33].

It is well-known that materials can have their properties considerably altered when subjected to extreme conditions [34]. The changes are highly dependent on their structural nature and the conditions applied to them. The high-velocity impact of nanostructures can give rise to a myriad of structural deformations, as it was demonstrated for the cases of nanotubes [35, 36] and nanoscrolls [37, 38]. This technique has even been considered a viable mechanism for synthesizing different materials with a whole different set of properties [34, 37]. To this date, however, a similar theoretical investigation

of the effects of the high-velocity impact of CNO is still lacking.

In this work, we carried out molecular dynamics simulations to investigate the high-velocity impact of CNO into a rigid substrate. To address these collision processes, we study in detail the structural, energetic, and stress aspects of these CNO/substrate impacts.

2. Methodology

We carried out fully atomistic reactive (ReaxFF) Molecular Dynamics simulations [40, 41] to investigate the impact of multi-shell CNO and their isolated shells (C_N fullerenes, where N stands for the number of atoms). Such simulations were conducted using the ReaxFF potential as implemented in the Large-scale Atomic/Molecular Massively Parallel Simulator (LAMMPS) [42]. The nanostructures obtained from reference [39] were edited to isolate the shells and smaller CNO using the Visual Molecular Dy-

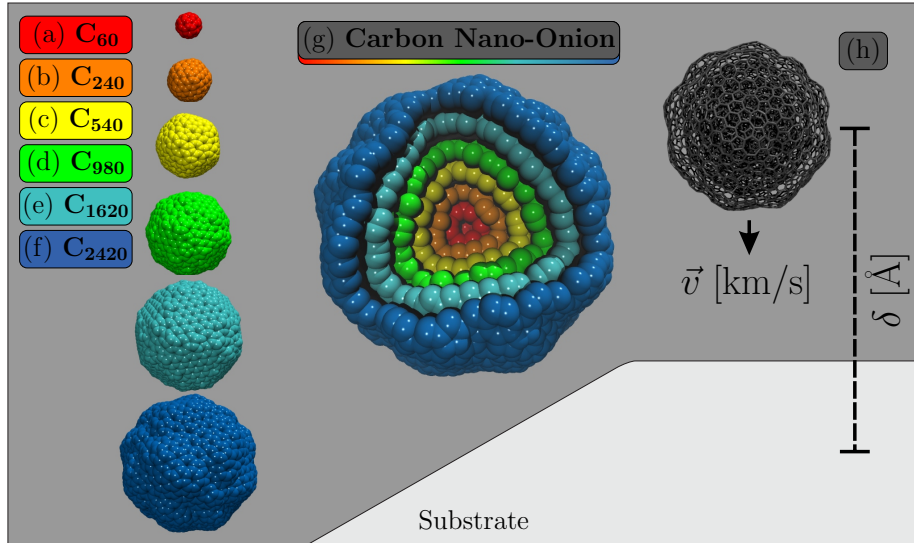


Figure 1: Schematic representation of the structural models of the carbon nano-onions used here. (a-f) illustrate the single structures (shells) that compose the full CNO, in which the number of carbon atoms varies from 60 up to 2420. The biggest multi-shell CNO has 5860 atoms. (g) depicts the composition of the CNO. (h) shows our initial simulation setup for the CNO/substrate system in which $\delta = 50 \text{ \AA}$. This CNO structure was created based on reference [39].

namics (VMD) software [43].

The typical CNO structure considered in this work is composed of an innermost shell of a C_{60} enclosed by a varying number — from two up to seven — of concentric buckyballs. In Figure 1 we present a schematic representation of a CNO with six shells, in which the number of carbon atoms varies from 60 up to 2420 atoms. The biggest multi-shell CNO has 5860 atoms. The CNO are formed by the composition of the different shells. The number of carbon atoms is included in the notation describing each CNO. As mentioned before, CNO_N corresponds to a CNO composed of a particular number of shells. N denotes the sum of the carbon atoms in these shells, from the smallest to the biggest fullerenes following the sequence shown in Figure 1 (e.g., CNO_{300} is a CNO composed by two shells: C_{60} and C_{240}). Our goal is to investigate the dynamics of the systems collision at different velocities with a fixed and rigid substrate. The CNO center of mass is initially placed 50 Å from the substrate.

The rigid substrate is considered using a fixed (time-independent) 12-6 Lennard-Jones potential. Such potential was parameterized using 10 Å cutoff distance, 0.07 Kcal/mol of interaction strength, and 3.55 Å distance between the particles for their interaction. We adopted a non-periodic unit cell with such repulsive potential between the nanostructures and the model substrate. We made use of a microcanonical (NVT) ensemble — to thermally equilibrate all structures at 300 K before the collision — and a microcanonical (NVE) ensemble [44] for simulating the impact, considering the fixed time step of 0.1 fs. The simulations were carried out during 10-50 ps, depending on the shooting velocity.

3. Results

The collision process of isolated shells and multi-shell CNO on a rigid substrate were investigated here. Each shell is a buckyball composed of between 60 to 2420 atoms. The multi-shell CNO considered in this work are composed of two up to seven shells, thus having from 300 up to 5860 carbon atoms, totaling 77 cases investigated, subjected to shooting velocities varying from 1.0 up to 7.0 Km/s.

The investigated systems were the following: As isolated shells, we considered C_{60} ,

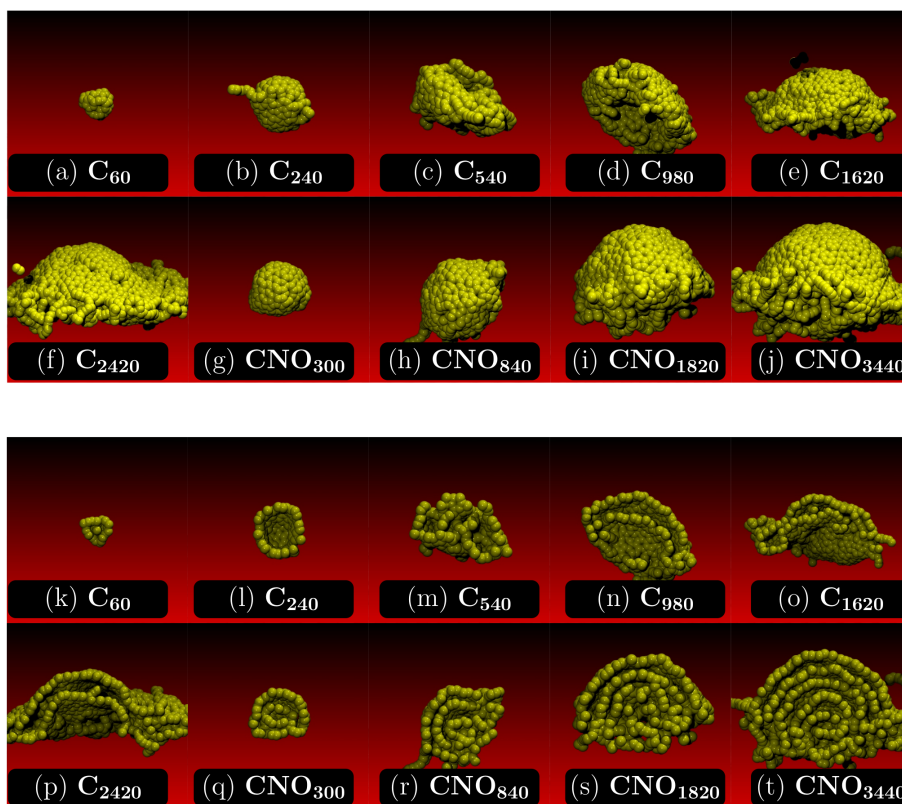


Figure 2: Representative MD snapshots for (a-f) the isolated shells and (g-j) for the CNO after their impacts. Here, CNO_N corresponds to a CNO composed of a particular number of shells. N denotes the sum of the carbon atoms in these shells, from the smallest to the largest fullerenes following the sequence shown in Figure 1 (e.g., CNO_{300} is a CNO composed by two shells: C_{60} and C_{240}). In these cases, the shooting velocity is 5.0 Km/s. (a-j) and (k-t) show front views and the corresponding cross-section views of the isolated shells, respectively.

C_{240} , C_{540} , C_{980} , C_{1620} and C_{2420} . Also, the following multi-shell CNO were studied: CNO_{300} (two shells: $C_{60} + C_{240}$), CNO_{840} (three shells: $CNO_{300} + C_{540}$), CNO_{1820} (four shells: $CNO_{840} + C_{940}$), CNO_{3340} (five shells: $CNO_{1820} + C_{1620}$), CNO_{5860} (six shells: $CNO_{3340} + C_{2420}$).

Figure 2 shows the representative MD snapshots (taken at 4.0 ps of simulation) for the impact of the fullerenes ranging from C_{60} up to CNO_{3440} , shooting velocity of 5.0 Km/s. The collisions occurred before this time for all cases. The figure is divided into

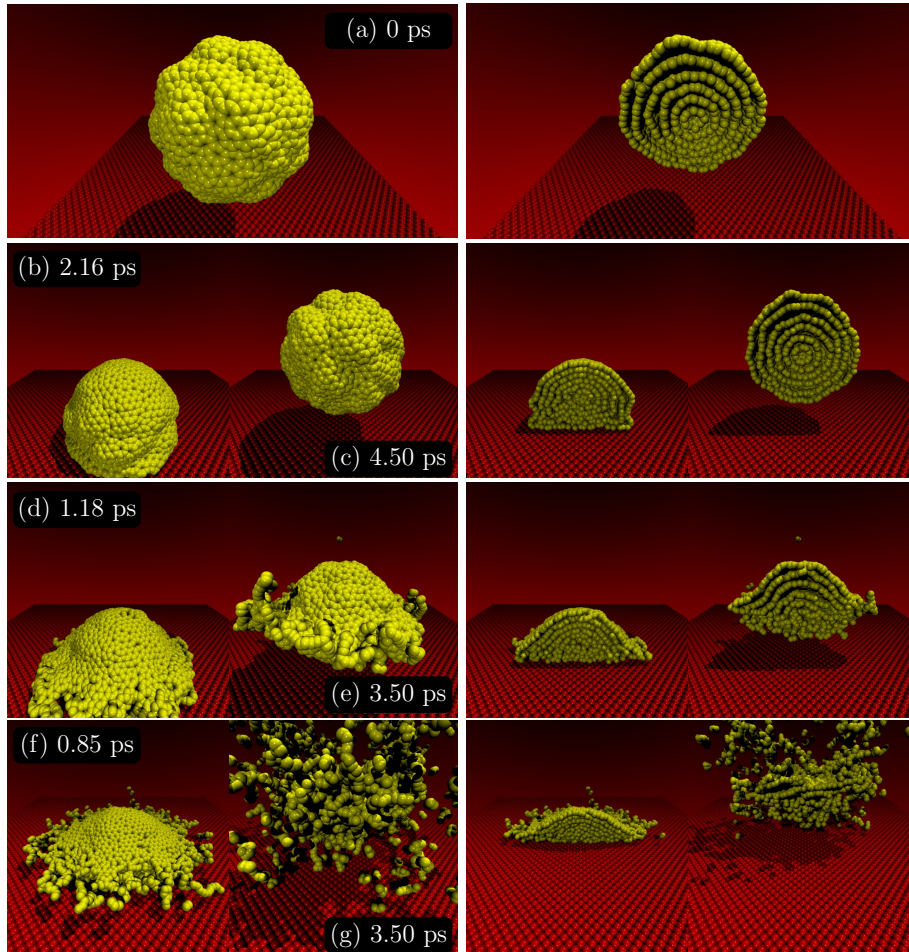


Figure 3: Representative MD snapshots for the multi-shell CNO (CNO_{5860}) impact at different shooting velocities: 2.0 Km/s (top panels), 5.0 Km/s (middle panels), 7.0 Km/s and (bottom panels). The left and right panels illustrate the front views and their corresponding cross-section views, respectively. The Supplementary Material shows the videos of the simulations for all the cases illustrated in this figure.

two panels. The upper panel shows a general view of the structure resulting from the collision. The lower one presents a cross-section view of the shells and multi-shell CNO to indicate the internal structural changes resulting from the impact. As a general trend, it is possible to observe that isolated shells possess very distinct deformation pattern dynamics. This trend is not true for the multi-shell CNO since the larger systems are less deformable than smaller ones.

We now discuss the case of the biggest multi-shell CNO considered in this work: CNO₅₈₆₀. In Figure 3, we compare the collisions results for 2.0, 5.0, and 7.0 Km/s shooting velocity values. The general and cross-section views are presented in the left and right panels, respectively. The chosen velocities are representative of three observed regimes. Supplementary Material shows the videos of the simulations for all the cases illustrated in this figure. At low velocities, up to 2 Km/s, we observed quasi-elastic collisions. This trend is clear comparing the original structure (Figure 3(a)) to the resulting ones (Figures 3(b) and 3(c)). At intermediate velocities, between 3.0 and 5.0 Km/s (see Figures 3(d) and 3(e)), inelastic collision occur, as evidenced by the substantial structural deformations. Finally, further increasing the velocities resulted in collapsed/fragmented structures, as can be seen in Figures 3(f) and 3(g). These regimes are similar to the ones reported for the cases of nanotubes [35, 36] and nanoscrolls [37, 38].

To gain further insights into the CNO collision mechanisms, we analyzed the stress per atom pattern (the von Mises Stress) during the impact (Figure 4), for the cases discussed in Figure 3 (the CNO₅₈₆₀ collision using 2.0 (Figures 4(b) and 4(c)), 5.0 (Figures 4(d) and 4(e)), and 7.0 Km/s (Figures 4(f) and 4(g)) as shooting velocities). In the color scheme adopted for this figure, white and red colors denote regions with null and maximum stress values per atom, respectively. The Von Mises stress is calculated accordingly to the procedure described in the reference [45]. In Figure 4(a), one can observe that the optimized structures of the model CNO used here are intrinsically stressed, as expected. At low velocities, up to 2 Km/s (Figures 4(b) and 4(c)), the stress per atom pattern does not change substantially after the collision. In this way, the quasi-elastic collisions can preserve regions with null stress (white regions). For the inelastic collisions, the CNO structure accumulates a significant amount of stress. Due to its topology, the stress accumulation is almost equally distributed over its surface after the collision, as illustrated in Figures 4(d-g). This trend for the distribution of the accumulated stress revealed that our model CNO does not present a most probable fracture point (or region). In carbon nanotubes, for instance, the stress accumulation during the impact can occur at the edge or in the center of the nanostructure yielding bilayer graphene or a graphene membrane, respectively [36].

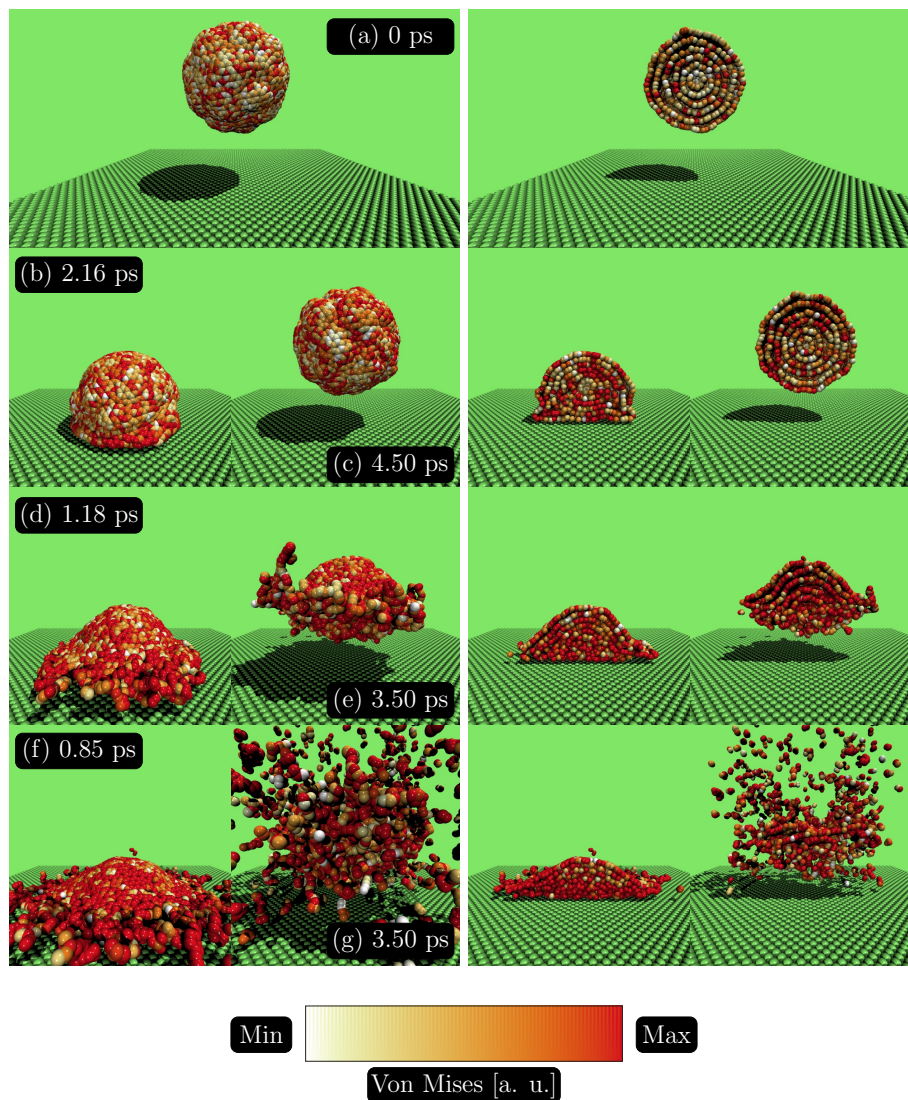


Figure 4: von Mises stress distribution as a function of the simulation time for the multi-shell CNO (CNO₅₈₆₀) impact at different shooting velocities: 2.0 Km/s (top panels), 5.0 Km/s (middle panels), 7.0 Km/s and (bottom panels). The left and right panels illustrate the front views and their corresponding cross-section views, respectively.

In Figure 5 we present the time evolution for the total number of different carbon-carbon bond types present in the CNO₅₈₆₀ structure. Figures 5(a), 5(b), and 5(c) shows the total number of bonds (sp^1 , sp^2 , and sp^3) for the impact of the nanostructure with

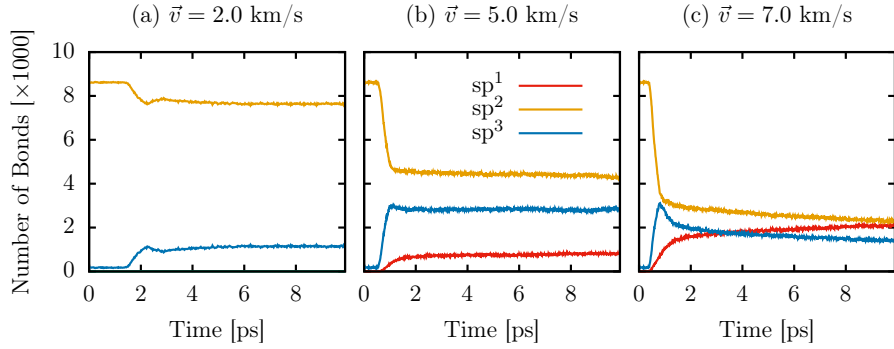


Figure 5: Time evolution for the total number of different carbon-carbon bond types of the CNO₅₈₆₀ system during the collision process.

initial velocities of 2.0, 5.0, and 7.0 Km/s, respectively. In Figure 5(a), one can observe that the initial CNO₅₈₆₀ configuration only presents sp^2 -like carbon-carbon bonds, as expected. At low velocities (up to 2 Km/s), almost 1000 bonds were converted from sp^2 -like to sp^3 -like ones after the quasi-elastic collision, as shown in Figure 5(a). The coexistence of sp^2 and sp^3 bond types remained until the end of the simulation, but with a predominance of sp^2 bonds, indicating only small CNO₅₈₆₀ structural deformations for low velocities. In this figure, a small number of sp^1 bonds were also observed due to the formation of linear atomic carbon chains (LACS) (see Figure 3(e)). For the high velocities regime (Figure 5(c)), the total number of sp^1 , sp^2 , and sp^3 bonds tend to be similar, but with a substantial decrease in the quantity of sp^1 and sp^2 bonds with relation to the two previous cases. The total number of sp^1 bonds increased due to a higher degree of fragmentation of the CNO₅₈₆₀ and subsequent LACS formation (see Figure 3(g)).

One striking result was the observation of the formation of a diamondoid-like core depending on the impact velocity. In Figures 6(a,c), we illustrate representative MD snapshots showing these cores for the shooting velocities of 5 and 7 Km/s. For the sake of clarity, the yellow bonds denote the diamondoid-like core, and their zoomed view is presented in the right panels, Figures 6(b,d). Interestingly, all the CNO shells contributed to the diamondoid-like core formation. This behavior is a relevant result.

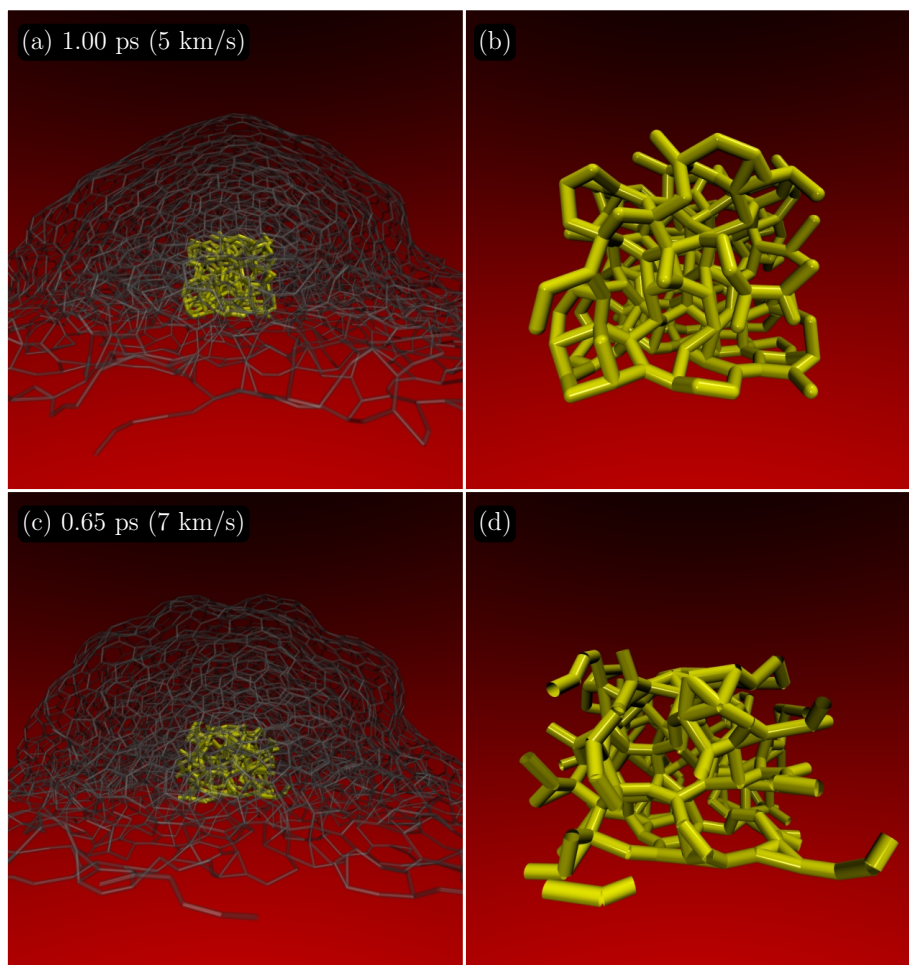


Figure 6: Representative MD snapshots illustrating the formation of diamondoids after the CNO_{5860} collision at (a-b) 5 Km/s and (c-d) 7 Km/s. For clarity, the yellow bonds illustrate the diamondoid-like cores, and their zoomed view is presented in the right panels (b-d).

It shows that under certain thermodynamic and/or internal pressure a diamondoid-like core can be formed in CNO. Although not always present in the experimentally realized CNO, some CNO with a diamondoid-like core has been experimentally observed [22].

Finally, in Figures 7(a-e), we present the kinetic and potential energy profiles as a function of the simulation time for the multi-shell CNO structures using 5 Km/s of shooting velocity as a representative case. Figure 7(f) shows the time required for con-

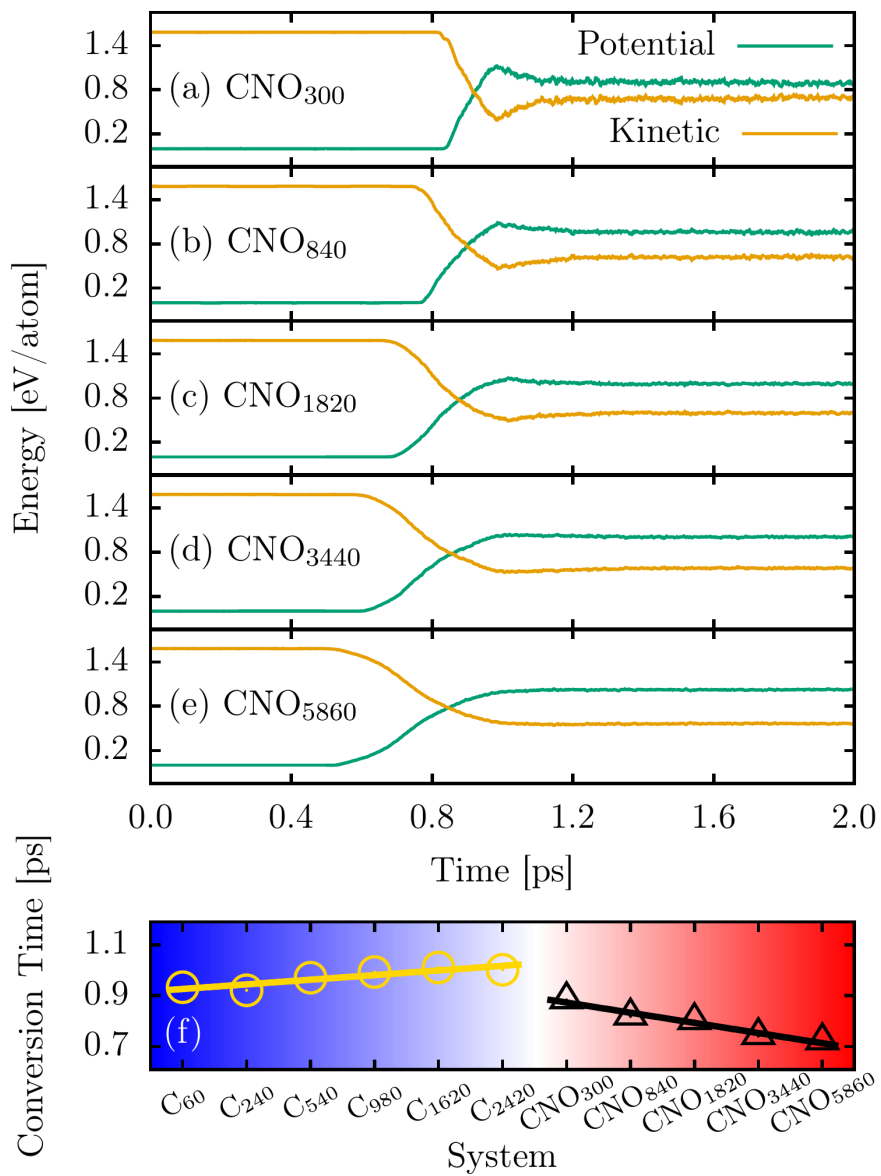


Figure 7: Kinetic and potential energy values as a function of the simulation time during the CNO collision, for the velocity case of 5 Km/s. At the bottom is also indicated compression time for the different structures.

verting kinetic into potential energy for the C_N (yellow line) and CNO_N (black line) cases. The total potential energy was shifted to zero by subtracting the CNO ground

state energy. In this sense, we are discussing the potential energy gain coming from the conversion of kinetic energy. Figure 7(f) presents the time required for the multi-shell CNO investigated here to convert their kinetic to potential energy (i.e., the conversion time during deformation). The CNO degree of deformability tends to increase when their size (i.e., the number of shells) increases. The CNO₃₀₀ and CNO₈₄₀ systems present an abrupt conversion between kinetic and potential energy (see Figures 7(a) and 7(b), respectively), that is related to the small size of the systems. For the CNO₁₈₂₀, CNO₃₄₄₀, and CNO₅₈₆₀ cases (see Figures 7(c), 7(d), and 7(e), respectively), the conversion between these energies occurs smoothly, despite their smaller deformability when contrasted to the CNO₃₀₀ and CNO₈₄₀ cases. The big CNO (Figures 7(a) and 7(b)) interact with the substrate earlier than the small ones (Figures 7(c-e)). Although the deformation levels are different between these CNO models, the amount of energy converted is independent of the system mass. We can see that the amount of energy converted was approximately 0.7 eV/atom for all cases. In the conversion process, the kinetic energy dropped from 1.6 to 0.7 eV/atom, while the potential energy acquired by the CNO after the collision increased from 0 to 0.9 eV/atom. Figure 7(f) shows that the conversion time has a linear trend for both C_N and CNO_N cases. In the C_N collision, the higher is the inner shell volume the greater is the conversion time, once the deformation degree of C_N shells increases with their volume. The CNO_N cases, in turn, presented an inverse trend. The higher is the system mass the smaller is the conversion time. The CNO_N stiffness increases with the number of shells, which makes the conversion between kinetic and potential energies faster.

4. Conclusions

In summary, we studied the dynamics and structural transformations of carbon onion-like structures under high-velocity impacts within the framework of fully atomistic reactive molecular dynamics simulations. We considered single and multi-shell nano-onions (up to six shells) and at different impact velocities (from 2 up to 7 Km/s) against a fixed and rigid substrate.

Our results showed the existence of three different regimes, depending on the im-

compact velocity: slightly deformed CNO (quasi-elastic collision), collapsed CNO (inelastic collisions) forming diamondoid-like cores, and fragmented CNO yielding LACS in a gas phase of carbon atoms. CNO tend to equally distribute through their surface the amount of accumulated stress during the collision.

The impact of CNO against the substrate yielded sp^3 -like bond types for all the used initial velocities. At intermediate velocities (between 3.0 and 5.0 Km/s), the inelastic collision forms diamondoid-like cores by converting a substantial quantity of sp^2 bonds into sp^3 ones. sp^1 bonds were also observed due to the formation of LACS. In the high velocities regime, the total number of sp^1 , sp^2 , and sp^3 bonds tend to be similar, around 2000. After the CNO impact and its subsequent fragmentation, the number of sp^1 bonds increases until the end of the simulation due to the formation of LACS.

Acknowledgments

The authors gratefully acknowledge the financial support from Brazilian research agencies CNPq, FAPESP, and FAP-DF. M.L.P.J gratefully acknowledges the financial support from CAPES grant 88882.383674/2019-01. D.S.G. thanks the Center for Computing in Engineering and Sciences at Unicamp for financial support through the FAPESP/CEPID Grants #2013/08293-7 and #2018/11352-7. L.A.R.J acknowledges the financial support from a Brazilian Research Council FAP-DF and CNPq grants 00193.0000248/2019 – 32 and 302236/2018 – 0, respectively. L.A.R.J acknowledges CENAPAD-SP for providing the computational facilities. L.A.R.J. gratefully acknowledges the financial support from IFD/UnB (Edital 01/2020) grant 23106.090790/2020–86. The authors acknowledge the National Laboratory for Scientific Computing (LNCC / MCTI, Brazil) for providing HPC resources of the SDumont supercomputer, which have contributed to the research results reported within this paper. URL: <http://sdumont.lncc.br>.

References

- [1] L. L. Zhang, X. Zhao, Carbon-based materials as supercapacitor electrodes, *Chemical Society Reviews* 38 (2009) 2520–2531.

- [2] K. P. Gopinath, D.-V. N. Vo, D. G. Prakash, A. A. Joseph, S. Viswanathan, J. Arun, Environmental applications of carbon-based materials: a review, *Environmental Chemistry Letters* 19 (2021) 557–582.
- [3] A. Kraft, A. C. Grimsdale, A. B. Holmes, Electroluminescent conjugated polymers—seeing polymers in a new light, *Angewandte Chemie International Edition* 37 (1998) 402–428.
- [4] S. Iijima, Helical microtubules of graphitic carbon, *nature* 354 (1991) 56–58.
- [5] M. Y. Han, B. Özyilmaz, Y. Zhang, P. Kim, Energy band-gap engineering of graphene nanoribbons, *Physical review letters* 98 (2007) 206805.
- [6] H. W. Kroto, J. R. Heath, S. C. O’Brien, R. F. Curl, R. E. Smalley, C 60: buckminsterfullerene, *nature* 318 (1985) 162–163.
- [7] H.-L. Zhang, J.-F. Li, B.-P. Zhang, K.-F. Yao, W.-S. Liu, H. Wang, Electrical and thermal properties of carbon nanotube bulk materials: Experimental studies for the 328–958 k temperature range, *Physical Review B* 75 (2007) 205407.
- [8] G. Keru, P. G. Ndungu, V. O. Nyamori, A review on carbon nanotube/polymer composites for organic solar cells, *International Journal of Energy Research* 38 (2014) 1635–1653.
- [9] C. Shuttle, B. O’Regan, A. Ballantyne, J. Nelson, D. D. Bradley, J. De Mello, J. Durrant, Experimental determination of the rate law for charge carrier decay in a polythiophene: Fullerene solar cell, *Applied Physics Letters* 92 (2008) 80.
- [10] X. Zhang, O. V. Yazyev, J. Feng, L. Xie, C. Tao, Y.-C. Chen, L. Jiao, Z. Pedramrazi, A. Zettl, S. G. Louie, et al., Experimentally engineering the edge termination of graphene nanoribbons, *ACS nano* 7 (2013) 198–202.
- [11] S. Dutta, S. K. Pati, Novel properties of graphene nanoribbons: a review, *Journal of Materials Chemistry* 20 (2010) 8207–8223.
- [12] Y. Ouyang, J. Guo, A theoretical study on thermoelectric properties of graphene nanoribbons, *Applied Physics Letters* 94 (2009) 263107.

- [13] D. Abergel, V. Apalkov, J. Berashevich, K. Ziegler, T. Chakraborty, Properties of graphene: a theoretical perspective, *Advances in Physics* 59 (2010) 261–482.
- [14] R. Bauernschmitt, R. Ahlrichs, F. H. Hennrich, M. M. Kappes, Experiment versus time dependent density functional theory prediction of fullerene electronic absorption, *Journal of the American Chemical Society* 120 (1998) 5052–5059.
- [15] M. A. Greaney, S. M. Gorun, Production, spectroscopy and electronic structure of soluble fullerene ions, *The Journal of Physical Chemistry* 95 (1991) 7142–7144.
- [16] F. Yao, D. T. Pham, Y. H. Lee, Carbon-based materials for lithium-ion batteries, electrochemical capacitors, and their hybrid devices, *ChemSusChem* 8 (2015) 2284–2311.
- [17] W. Lv, Z. Li, Y. Deng, Q.-H. Yang, F. Kang, Graphene-based materials for electrochemical energy storage devices: opportunities and challenges, *Energy Storage Materials* 2 (2016) 107–138.
- [18] P. Trogadas, T. F. Fuller, P. Strasser, Carbon as catalyst and support for electrochemical energy conversion, *Carbon* 75 (2014) 5–42.
- [19] J. Wang, H. L. Xin, D. Wang, Recent progress on mesoporous carbon materials for advanced energy conversion and storage, *Particle & particle systems characterization* 31 (2014) 515–539.
- [20] D. Ugarte, Curling and closure of graphitic networks under electron-beam irradiation, *Nature* 359 (1992) 707–709.
- [21] M. Zeiger, N. Jäckel, V. N. Mochalin, V. Presser, carbon onions for electrochemical energy storage, *Journal of Materials Chemistry A* 4 (2016) 3172–3196.
- [22] F. Banhart, P. M. Ajayan, Carbon onions as nanoscopic pressure cells for diamond formation, *Nature* 382 (1996) 433–435.
- [23] J. Bartelmess, S. Giordani, Carbon nano-onions (multi-layer fullerenes): chemistry and applications, *Beilstein journal of nanotechnology* 5 (2014) 1980–1998.

- [24] L.-C. Qin, S. Iijima, Onion-like graphitic particles produced from diamond, *Chemical physics letters* 262 (1996) 252–258.
- [25] M. Ghosh, S. K. Sonkar, M. Saxena, S. Sarkar, Carbon nano-onions for imaging the life cycle of *drosophila melanogaster*, *Small* 7 (2011) 3170–3177.
- [26] S. K. Sonkar, M. Ghosh, M. Roy, A. Begum, S. Sarkar, Carbon nano-onions as nontoxic and high-fluorescence bioimaging agent in food chain—an in vivo study from unicellular *e. coli* to multicellular *c. elegans*, *Materials Express* 2 (2012) 105–114.
- [27] J. Luszczyn, M. E. Plonska-Brzezinska, A. Palkar, A. T. Dubis, A. Simionescu, D. T. Simionescu, B. Kalska-Szostko, K. Winkler, L. Echegoyen, Small nontoxic carbon nano-onions: first covalent functionalization with biomolecules, *Chemistry—A European Journal* 16 (2010) 4870–4880.
- [28] M. B. Seymour, C. Su, Y. Gao, Y. Lu, Y. Li, Characterization of carbon nano-onions for heavy metal ion remediation, *Journal of Nanoparticle Research* 14 (2012) 1–13.
- [29] F.-D. Han, B. Yao, Y.-J. Bai, Preparation of carbon nano-onions and their application as anode materials for rechargeable lithium-ion batteries, *The Journal of Physical Chemistry C* 115 (2011) 8923–8927.
- [30] D. Su, N. I. Maksimova, G. Mestl, V. L. Kuznetsov, V. Keller, R. Schlögl, N. Keller, Oxidative dehydrogenation of ethylbenzene to styrene over ultra-dispersed diamond and onion-like carbon, *Carbon* 45 (2007) 2145–2151.
- [31] T. Cabioch, E. Thune, J. Riviere, S. Camelio, J. Girard, P. Guerin, M. Jaouen, L. Henrard, P. Lambin, Structure and properties of carbon onion layers deposited onto various substrates, *Journal of applied physics* 91 (2002) 1560–1567.
- [32] E. Koudoumas, O. Kokkinaki, M. Konstantaki, S. Couris, S. Korovin, P. Detkov, V. Kuznetsov, S. Pimenov, V. Pustovoi, Onion-like carbon and diamond nanoparticles for optical limiting, *Chemical physics letters* 357 (2002) 336–340.

- [33] S. Sek, J. Breczko, M. E. Plonska-Brzezinska, A. Z. Wilczewska, L. Echegoyen, Stm-based molecular junction of carbon nano-onion, *ChemPhysChem* 14 (2013) 96–100.
- [34] E. F. Oliveira, P. A. da Silva Autreto, D. S. Galvão, On hardening silver nanocubes by high-velocity impacts: a fully atomistic molecular dynamics investigation, *Journal of materials science* 53 (2018) 7486–7492.
- [35] S. Ozden, P. A. Autreto, C. S. Tiwary, S. Khatiwada, L. Machado, D. S. Galvao, R. Vajtai, E. V. Barrera, P. M. Ajayan, Unzipping carbon nanotubes at high impact, *Nano letters* 14 (2014) 4131–4137.
- [36] E. Armani, P. A. Autreto, High-velocity impact of a hybrid cbn nanotubes, *Oxford Open Materials Science* 1 (2021) itaa006.
- [37] C. F. Woellner, L. D. Machado, P. A. Autreto, J. M. de Sousa, D. S. Galvao, Structural transformations of carbon and boron nitride nanoscrolls at high impact collisions, *Physical Chemistry Chemical Physics* 20 (2018) 4911–4916.
- [38] J. M. de Sousa, L. D. Machado, C. F. Woellner, P. A. da Silva Autreto, D. S. Galvao, Carbon nanoscrolls at high impacts: A molecular dynamics investigation, *MRS Advances* 1 (2016) 1423–1428.
- [39] H. Qi, S. Picaud, M. Devel, E. Liang, Z. Wang, Adsorption of organic molecules on onion-like carbons: insights on the formation of interstellar hydrocarbons, *The Astrophysical Journal* 867 (2018) 133.
- [40] A. C. Van Duin, S. Dasgupta, F. Lorant, W. A. Goddard, Reaxff: a reactive force field for hydrocarbons, *The Journal of Physical Chemistry A* 105 (2001) 9396–9409.
- [41] C. Ashraf, A. C. Van Duin, Extension of the reaxff combustion force field toward syngas combustion and initial oxidation kinetics, *The Journal of Physical Chemistry A* 121 (2017) 1051–1068.

- [42] S. Plimpton, Fast parallel algorithms for short-range molecular dynamics, *J. Comput. Phys.* 117 (1995) 1–19.
- [43] W. Humphrey, A. Dalke, K. Schulten, et al., Vmd: visual molecular dynamics, *Journal of molecular graphics* 14 (1996) 33–38.
- [44] W. G. Hoover, Canonical dynamics: equilibrium phase-space distributions, *Physical review A* 31 (1985) 1695.
- [45] L. C. Felix, R. M. Tromer, P. A. Autreto, L. A. Ribeiro Junior, D. S. Galvao, On the mechanical properties and thermal stability of a recently synthesized monolayer amorphous carbon, *The Journal of Physical Chemistry C* 124 (2020) 14855–14860.